

Supplementary Information (SI)

Iron Phosphide Encapsulated in P-doped Graphitic Carbon as Efficient and Stable Electrocatalyst for Hydrogen and Oxygen Evolution Reactions

Yunduo Yao^{a,b}, Nasir Mahmood^{b,c}, Lun Pan^{a,b}, Guoqiang Shen^{a,b}, Rongrong Zhang^{a,b}, Ruijie Gao^{a,b}, Fazal-e-Aleem^d, Xiaoya Yuan^e, Xiangwen Zhang^{a,b}, Ji-Jun Zou^{a,b*}

^aKey Laboratory for Green Chemical Technology of Ministry of Education, School of Chemical Engineering and Technology, Tianjin University, Tianjin 300072, China.

^b Collaborative Innovative Center of Chemical Science and Engineering (Tianjin), Tianjin 300072, China.

^c School of Engineering, RMIT University, 124 La Trobe Street, 3001 Melbourne, Victoria, Australia.

^d Department of Physics, The University of Lahore, 1-Km, Raiwind Road, Lahore, 54600, Pakistan.

^e College of Materials Science and Engineering, Chongqing Jiaotong University, Chongqing 400074, China.

*E-mail: jj_zou@tju.edu.cn

Experimental Section

Reagents. Iron (III) chloride (FeCl_3 , 99.9%), 1,4-benzenedicarboxylic acid (1, 4-BDC, 98%), N,N-dimethylformamide (DMF, AR), sodium hypophosphite (NaH_2PO_2 , 99%), potassium hydroxide (KOH, 99.99%) were obtained from Aladdin Industrial Inc. (Shanghai China). Sulfuric acid (H_2SO_4), ethanol ($\text{C}_2\text{H}_5\text{OH}$, AR) was obtained from Real&Lead Chemical Co.Ltd (Tianjin China). Commercial platinum on carbon (Pt/C, 10 wt%), ruthenium (IV) oxide (RuO_2), iridium (IV) oxide (IrO_2), conductive carbon (Vulcan XC-72R) and nafion solution (5% wt) were obtained from Sigma-Aldrich. All reagents in this work were used as received without further purification. Ultrapure Milli-Q water (resistivity > 18.2 M Ω cm) was used in all experiments.

Synthesis of catalysts.

Synthesis of Fe-MIL-88

The synthesis method of Fe-MIL-88 was similar to other reported literatures except for a few improvements.¹ Briefly, 1,4-BDC (1.384mmol, 224.5 mg) and FeCl_3 (1.384mmol, 229.9. mg) were dissolved in 30mL DMF under magnetic stirring until homogeneous yellow solution obtained. Then the above mixture solution was transferred in an oil bath at 120 °C for 4h. After cooling to room temperature naturally, the products were collected and washed via centrifugation with DMF, ethanol and water three times, respectively, then dried at 60 °C overnight.

Pyrolysis step

The orange powders Fe-MIL-88 were transferred to a covered crucible, heated to 800 or 850°C at a rate of 2 °C/min and maintained at settled temperature for 2 h in tube furnace under N_2 atmosphere. Then the black powder was collected directly after cooling down to room temperature without further treatment and named as Fe@GC-800 or Fe@GC-850 according to pyrolysis temperature.

Phosphorization step

The as-synthesized black powder Fe@GC mixed with NaH_2PO_2 as a mass ratio of 1:20 and grinded sufficiently. Then, the resulted uniform powder was annealed at 300, 325 or 350 °C for 2 h with heating rate of 1 °C/min in tube furnace under N_2 atmosphere. Finally, the obtained grey powder was washed via centrifugation with water and ethanol more than ten times until impurities completely removing, and then dried in vacuum oven at 60 °C overnight.

To synthesis $\text{Fe}_2\text{P}@APC$, the procedure is almost the same as with the above one, except the addition of the same amount of precursor Fe-MIL-88 as that in pyrolysis step to replace Fe@GC.

Synthesis of GPC

Briefly, phytic acid aqueous solution (50 w/w%) was placed in 100 mL glass beaker and then heated under 180 °C for 16 h for polymerization, then the black polymer (solid) was carbonized at

900 °C in tube furnace under N₂ atmosphere for 1 h.

Electrochemical measurements. Electrochemical tests were evaluated using an IviumStat electrochemical workstation (Ivium Technologies BV, Netherlands) in a typical three-electrode setup, where graphite rod was used as the counter electrode, glassy carbon electrode (GCE, 3 mm in diameter) modified by catalyst as the working electrode and mercury oxide mercury electrode (Hg/HgO, 1.0 M KOH) or a saturated calomel electrode (SCE, saturated KCl) as the reference electrode in 1.0 M KOH or 0.5 M H₂SO₄ electrolyte at room temperature, respectively. Prior to each test, GCE was polished on a polishing cloth using alumina pastes to obtain a mirror-like surface, followed by ultrasonic cleaning in ethanol and water. Then the catalyst suspension ink was prepared by dispersing 5 mg catalyst and 1 mg conductive carbon powder in 1 mL of solution containing 700 μL water, 270 μL ethanol as well as 30 μL Nafion solution, followed by ultrasonication for hours. To modify the working electrode, 5 μL of the ink was drop-casted onto a GCE, and then dried at room temperature naturally to form a catalyst film with mass loading of ~0.35 mg cm⁻².

The linear sweep voltammetry (LSV) curves in each electrolyte (O₂-saturated 1.0 M KOH and or N₂-saturated 0.5M H₂SO₄ solution) were measured at a scan rate of 5 mV s⁻¹. The electrochemical impedance spectra (EIS) was recorded at the overpotential of -0.1 V vs. RHE for HER and 0.3 V vs. RHE for OER, respectively at related frequencies ranged from 100 kHz to 0.01 Hz with a 5 mV amplitude. The stability was evaluated separately by two different methods to cross check for various electrodes. One is re-measured LSV results after cyclic voltammetry (CV) for 3000 cycles. The other is current-time dependent stability test performed at a constant overpotential to drive the current density of 10 mA cm⁻². The potentials recorded from electrochemical measurements were all calibrated to the reversible hydrogen electrode (E_{RHE}) following the two equation: E_{RHE}=E_{SCE}+0.0591×pH+0.242 or E_{RHE}=E_{Hg/HgO}+ 0.0591×pH+0.12, where E_{SCE} and E_{Hg/HgO} were potentials directly measured with SCE or Hg/HgO reference electrode. Except the LSV and tafel curves, other test results were directly used without *iR*-compensation. For all of half-cell electrochemical measurements, the electrodes were cycled at 50 mV s⁻¹ until reproducible CVs were obtained.

Catalytic parameter calculations

Tafel slope and exchange current density (*j*₀) were calculated by Tafel curves, which were plotted by using the equation:

$$\eta = a + b \log|j|$$

where η is the overpotential, j is the current density, a is the intercept and b is the Tafel slope.

It can be as one of important factors to indicate the reaction kinetics and mechanism as well as define the rate-determining step.² As suggested by classic two-electron-reaction models, the HER process undergoes a two-step reaction process, which is suggested as two different mechanisms with three possible reactions: a discharge step (Volmer reaction: $\text{H}_3\text{O}^+ + \text{M} + \text{e}^- \rightarrow \text{H}_{\text{ads}} + \text{H}_2\text{O}$) followed by a desorption step (Heyrovsky reaction: $\text{H}_{\text{ads}} + \text{H}_3\text{O}^+ + \text{e}^- \rightarrow \text{H}_2 + \text{M} + \text{H}_2\text{O}$) or a recombination step (Tafel reaction: $\text{H}_{\text{ads}} + \text{H}_{\text{ads}} \rightarrow \text{H}_2 + \text{M}$), where H_{ads} represents the intermediate state of an adsorbed hydrogen atom on the active site of the catalyst.³ The rate-determining step in the HER process might be the Volmer, Heyrovsky, or Tafel reaction with the corresponding characteristic Tafel slopes of 120, 40, or 30 mV dec⁻¹.

Exchange current density (j_0) was evaluated by extrapolation to the Tafel curve to $\eta = 0$. It is the intrinsic property of the electrode reaction, which depends only on catalyst materials, electrolyte and temperature. Electrode reaction with higher exchange current density needs less driving force to promote the reaction, suggesting better activity.

Electrochemical active surface area (ECSA): The electrochemical capacitive currents were measured by simple CV method within a non-Faradaic region (from 0.10-0.20 V vs. RHE for HER and from 1.0-1.10 V vs. RHE for OER) for twenty circles at each of five different scan rates (10, 20, 30, 40 and 50 mV s⁻¹). The differences in current density variation ($\Delta j = j_a - j_c$) at the potential of 0.15 V or 1.05 V vs RHE plotted against scan rate are linear fitted to estimate the slope, which is twice of electrochemical double-layer capacitances (C_{dl}). In the end, ECSA was calculated by the double layered capacitance (C_{dl}) using the specific capacitance value for a flat standard with 1 cm² of real surface area by following equation⁴:

$$\text{ECSA} = C_{\text{dl}}/C_s$$

where the specific capacitance for a flat surface (C_s) of our materials are used as 40 μF cm⁻², as reported in other articles.⁵

Turnover Frequency Calculations (TOFs): TOF was calculated by following equation⁴:

$$\text{TOF} = \frac{\text{the number of total hydrogen turnovers/cm}^{-2} \text{ of geometric area}}{\text{the number of active sites/cm}^{-2} \text{ of geometric area}}$$

The total number of hydrogen turn overs (*No. of H₂*) was calculated from the current density according to:

$$\text{No. of H}_2 = j \left(\frac{\text{mA}}{\text{cm}^{-2}} \right) \left(\frac{1 \text{ C s}^{-1}}{1000 \text{ mA}} \right) \left(\frac{1 \text{ mol of e}^{-1}}{2 \text{ mol of e}^{-1}} \right) \left(\frac{6.02 \times 10^{23} \text{ H}_2 \text{ molecules}}{1 \text{ mol of H}_2} \right) =$$

$$3.12 \times 10^{15} \frac{\text{H}_2/\text{s}}{\text{cm}^{-2}} \text{ per } \frac{\text{mA}}{\text{cm}^{-2}}$$

The active sites per real surface area ((No. of active sites) calculated from the following formula:

$$\text{No. of active sites} = \left(\frac{\text{No. of atoms/unit cell}}{\text{Volume/unit cell}} \right)^{2/3}$$

Finally, the plot of current density can be converted into a TOF plot according to the following formula:

$$\text{TOF} = \frac{\left(3.12 \times 10^{15} \frac{\text{H}_2/\text{s}}{\text{cm}^{-2}} \text{ per } \frac{\text{mA}}{\text{cm}^{-2}} \right) \times |j|}{\text{No. of active sites} \times \text{ECSA}}$$

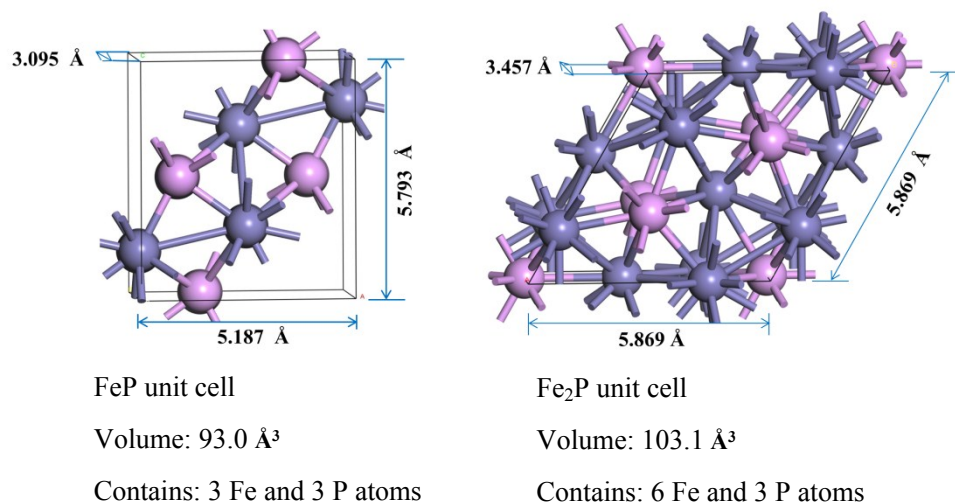


Figure S1. Fe₂P and FeP unit cells. Fe atoms: dark purple and P atoms: light purple

Since the exact cell parameters for composite Fe₂P/FeP@GPC are not known and the surface sites of Fe₂P and FeP are similar, we estimated the number of active sites as the number of surface sites (including both Fe and P atoms as possible active sites) from the average value of Fe₂P and FeP as early report.⁶ Furthermore, *j* is applied at the potential of -100 mV for all catalysts.

Characterizations. Surface morphologies of catalysts were examined by scanning electron microscope (SEM) using a Hitachi S-4800 instrument. Transmission electron microscopy (TEM), high-resolution transmission electron microscopy (HRTEM) and elemental mapping were performed on Tecnai G2 F20 transmission electron microscope at 200 kV. The crystal structures were recorded on a Rigaku D/max-2500 X-ray diffractometer (XRD) equipped with Cu K α irradiation source ($\lambda = 0.1542$ nm) (40 kV and 40 mA). Elemental composition and bonding information was analyzed with an X-ray photoelectron spectroscopy (XPS) operated at a pass

energy of 187.85 eV (Physical Electronics PHI 1600 ESCA XPS system with monochromated Al $K\alpha$ X-ray source) and corrected by taken the C 1s peak at 284.8 eV as internal standard. Raman spectra were recorded using a Raman spectrometer (DXR Microscope) and a green semiconductor laser (532 nm) as excitation source. Nitrogen adsorption-desorption isotherm was analyzed with ASAP 2020 physisorption Analyzer at 77 K. Before performing the measurement, the sample was outgassed under vacuum at 200 °C for 12 h until the pressure was less than 0.66 Pa. The specific surface area was calculated by the conventional Brunauer-Emmett-Teller (BET) method. Pore size distribution was determined by Barrett-Joyner-Halenda (BJH) method.

S2. Supplemental figures and tables

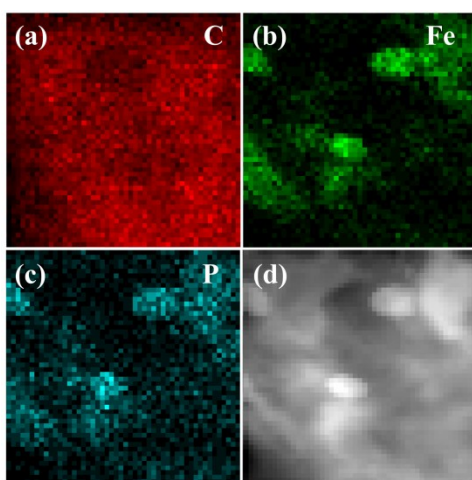


Figure S2.Elemental mapping image of Fe@GC-800.

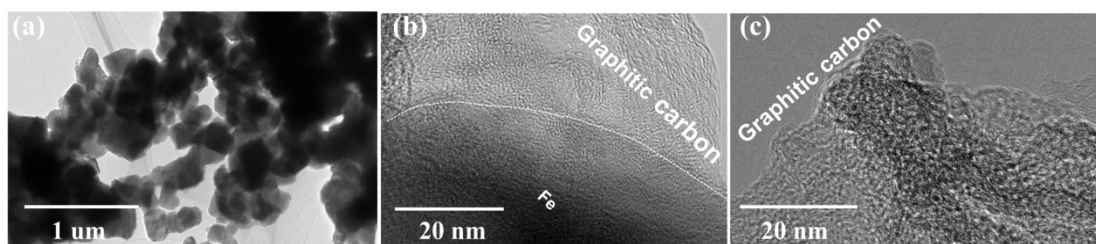


Figure S3. TEM and HRTEM images of Fe@GC-850.

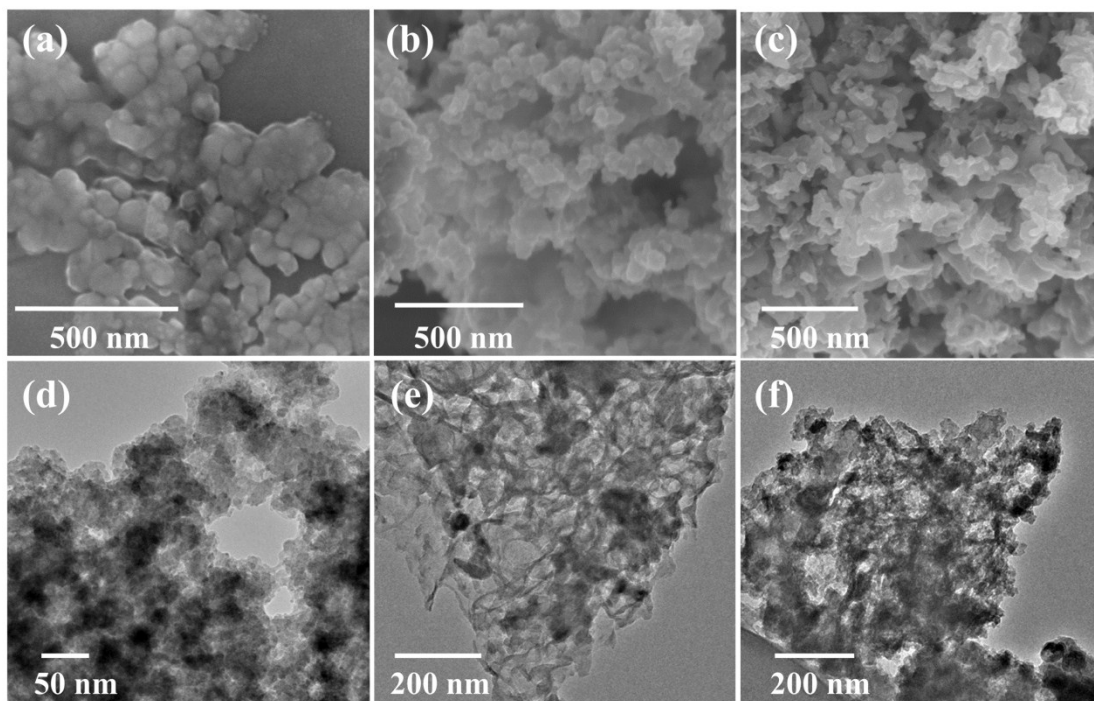


Figure S4. SEM and TEM image of (a) (d) Fe₂P@APC, (b) (e) FeP@GPC and (c) (f) Fe₂P/FeP@GPC, respectively.

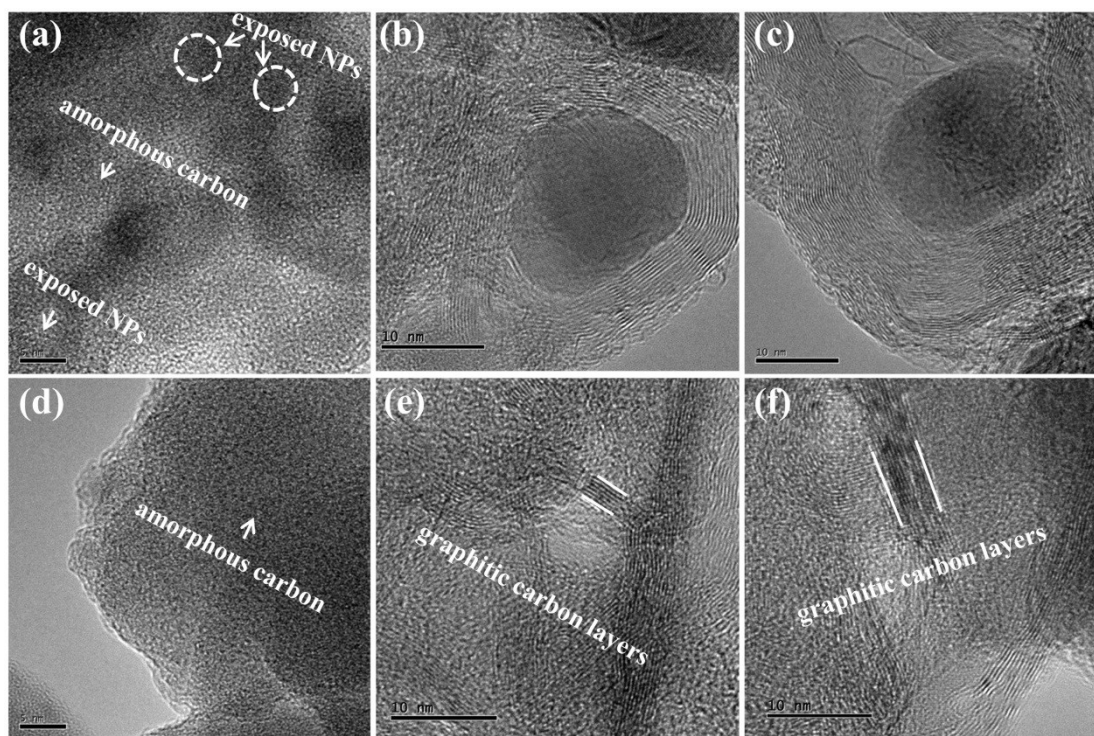


Figure S5. HRTEM images of (a) (d) Fe₂P@APC, (b) (e) FeP@GPC and (c) (f) Fe₂P/FeP@GPC.

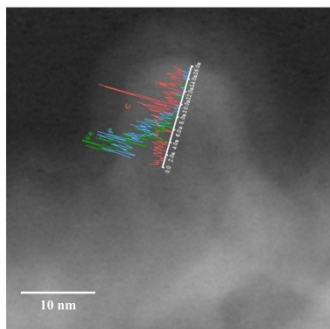


Figure S6. EDX line-scan profiles with Fe, P and C K shells of FeP@GPC catalyst.

Table S1. The element analysis results by EDX, XPS and ICP

Catalyst	EDX (Atomic %)				XPS (Atomic %)				ICP							
	Fe	P	C	P/Fe	Fe	P	C	P/Fe	(Atomic %)				(Massive %)			
	Fe	P	C	P/Fe	Fe	P	C	P/Fe	Fe	P	C	P/Fe	Fe	P	C	P/C
Fe ₂ P@APC	5.17	21.05	73.76	4.07	6.75	40.22	53.03	5.96	6.57	18.39	75.04	2.80	20.00	31.01	48.99	0.633
Fe ₂ P/FeP@GPC	29.40	46.76	23.84	1.59	4.66	27.55	67.79	5.91	6.79	10.51	82.70	1.55	22.39	19.18	58.43	0.328
FeP@GPC	12.41	15.02	72.57	1.21	4.36	22.97	72.67	5.27	3.98	9.88	86.14	2.48	14.26	19.60	66.14	0.296

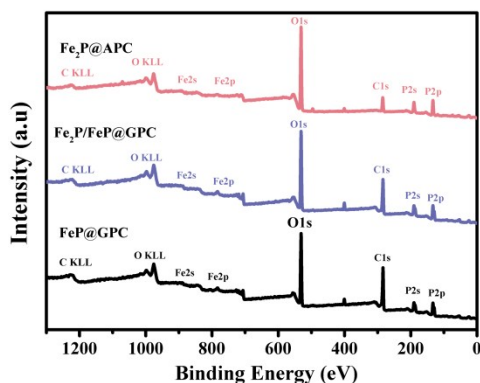


Figure S7. Full scan XPS spectra of Fe₂P@APC, Fe₂P/FeP@GPC and FeP@GPC.

Table S2. Binding energy information from the fitted Fe 2p and P 2p spectra of Fe-P bond in as-synthesized catalysts.

Catalyst	2p _{3/2} (B.E.)/eV		2p _{1/2} (B.E.)/eV	
	Fe ^{δ+}	P ^{δ-}	Fe ^{δ+}	P ^{δ-}
Fe ₂ P@APC	707.20	129.50	720.15	130.21
Fe ₂ P/FeP@GPC	707.38	129.47	720.25	130.20
FeP@GPC	707.63	129.40	720.33	130.10

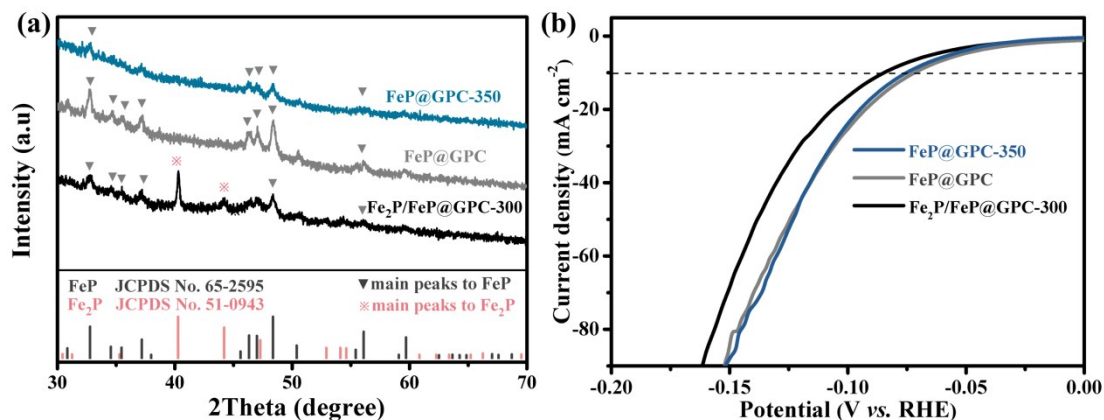


Figure S8. (a) XRD results (b) HER electrocatalytic activity measured in 0.5 M H₂SO₄ solution of a series of Fe₂P/FeP@GPC catalysts under the same pyrolysis condition but different phosphorization temperature at 300, 325 and 350 °C, respectively.

Note: After phosphorization of Fe@GC-800 at different temperature, the as-synthesized catalyst at lower temperature (300°C) was composed of a mixture of Fe₂P (JCPDS No. 51-0943) and FeP (JCPDS No. 65-2595) referred as Fe₂P/FeP@GPC-300, performing lowest HER activity. When the temperatures increased to 325 or 350 °C, pure FeP phase catalysts were obtained with similarly best activity according to **Figure S8** referred as FeP@GPC or FeP@GPC-350, which implies that FeP is more active to facilitate HER than Fe₂P in H₂SO₄ solution.

Table S3. The summarization for HER characteristics of all-synthesized catalysts

Catalyst	η_{10} (mV) ^a	Tafel slope (mV dec ⁻¹) ^b	j_0 (mA cm ⁻²) ^c	R_{ct} (Ω) ^d	C_{dl} (mF cm ⁻²) ^e	ECSA (cm ²) ^f	TOF (s ⁻¹)
Fe@GC	--	225	0.021	10000	0.055	1.375	--
Fe ₂ P@APC	196	90	0.066	1126	0.330	8.25	0.127
FeP@GPC	72	68	0.059	22.3	2.240	56	0.952
Fe ₂ P/FeP@GPC	205	92	0.871	1301	0.315	7.875	0.119

^a) Obtained from polarization curves of HER in 0.5 M H₂SO₄ at the current density of 10 mA cm⁻² over the different as-synthesized materials;

^{b,c}) Obtained from Tafel curves according to Tafel equation;

^d) Obtained from the EIS results fitted with electrical equivalent circuit model;

^e) Obtained from the linear graphs of Δj ($j_a - j_c$) at 0.15 V vs the scan rate, in which the slopes represent twice the values of C_{dl} ;

^f) Estimated from the following equation: $ECSA \approx C_{dl}/C_s$;

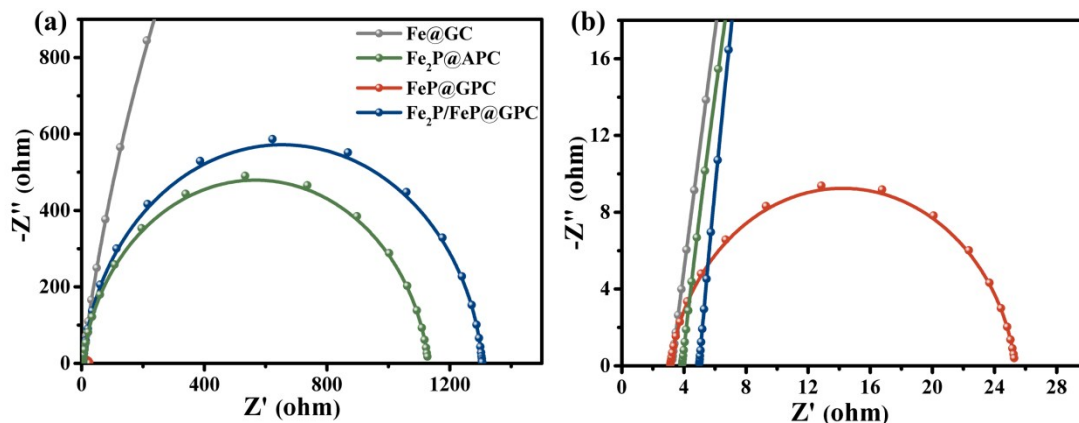


Figure S9. Nyquist curves derived from EIS measurements for HER, showing lowest charge-transfer resistance of FeP@GPC.

Table S4. EIS results fitted with electrical equivalent circuit model

Catalyst	R_s (Ω)	R_{ct} (Ω)	Q (mF)	n
Fe@GC	3.2	10000	$1.80 \cdot 10^{-5}$	0.90
Fe ₂ P@APC	3.8	1126	$5.02 \cdot 10^{-5}$	0.91
FeP@GPC	3.2	22.3	$3.66 \cdot 10^{-4}$	0.90
Fe ₂ P/FeP@GPC	5.0	1301	$2.60 \cdot 10^{-5}$	0.94

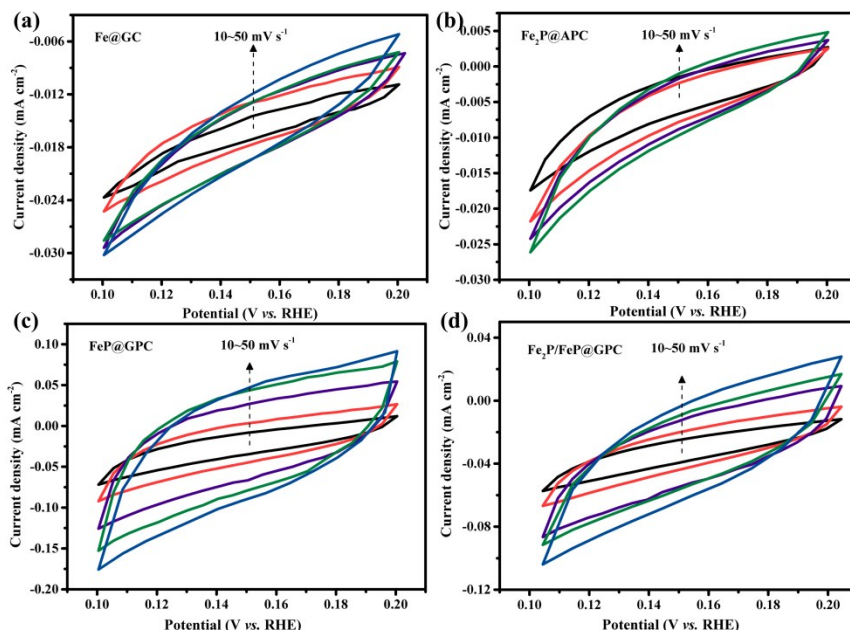


Figure S10. Cyclic voltammograms (CV) curves in 0.5 M H₂SO₄ for (a) Fe@GC, (b) Fe₂P@APC, (d) FeP@GPC, (e) Fe₂P/FeP@GPC in the region of 0.10–0.20 V vs. RHE at various scan rates.

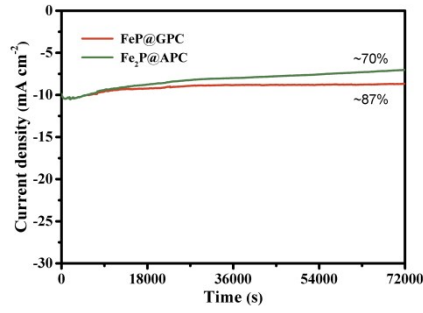


Figure S11 Chronoamperometric curves of as-synthesized Fe₂P@APC and FeP@GPC at applied constant overpotential of 196 mV and 72 mV vs RHE for 20h, respectively.

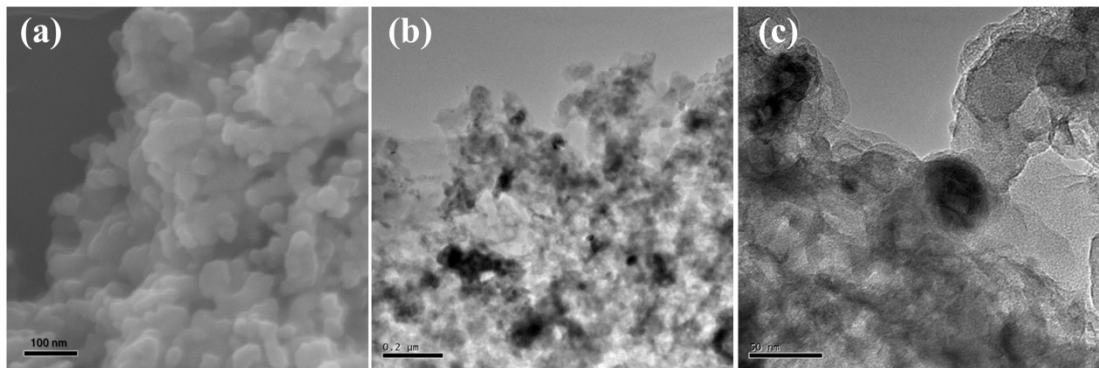


Figure S12 (a) SEM and (b) (c) TEM images of FeP@GPC after long time stability testing for HER in 0.5 M H₂SO₄.

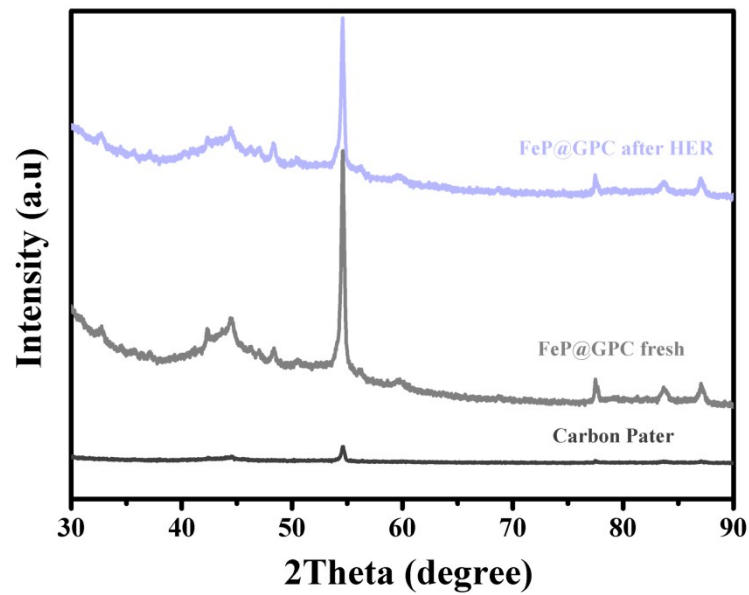


Figure S13 XRD results of FeP@PC-800 coating on carbon paper before and after long time stability testing for HER in 0.5 M H₂SO₄.

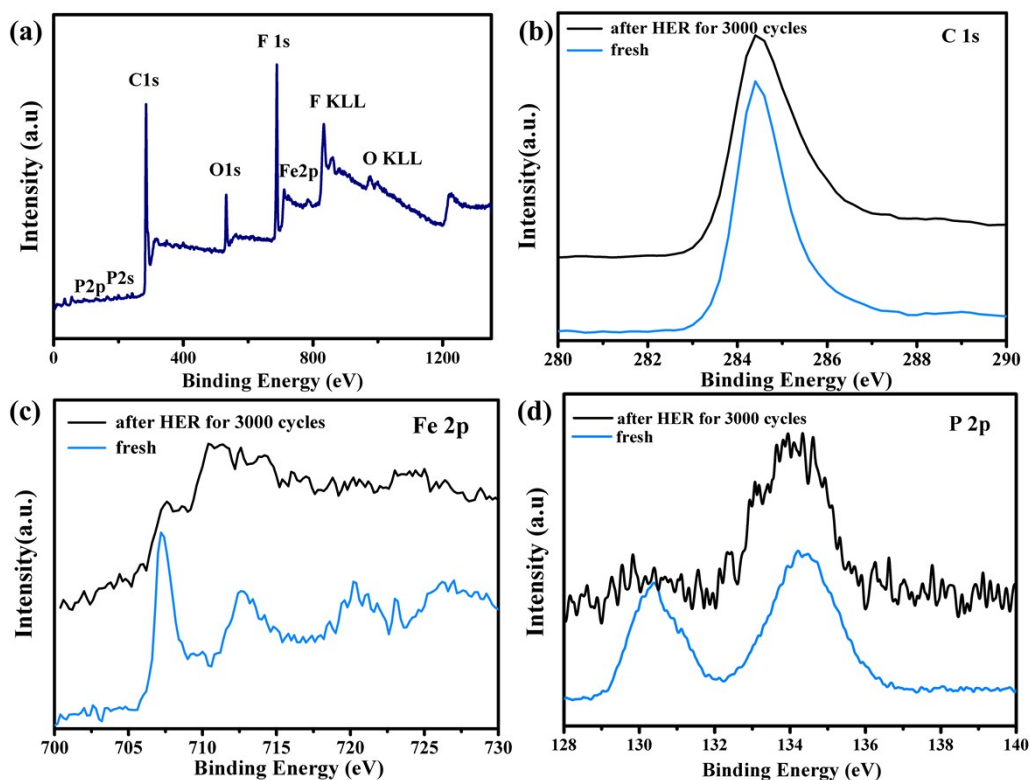


Figure S14 XPS results of FeP@GPC coating on carbon paper before and after long time stability testing for HER in 0.5M H₂SO₄.

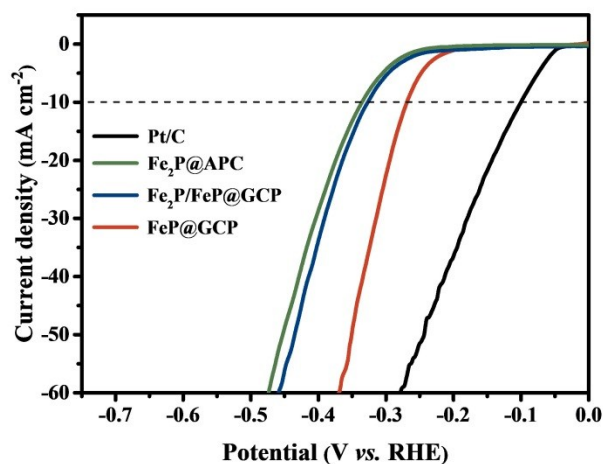


Figure S15. HER electrocatalytic activity measured in 1 M KOH solution.

Table S5. The summarization for OER characteristics of all the synthesized catalysts.

Catalyst	η_{10} (mV) ^a	Tafel slope (mV dec ⁻¹) ^b	R_{ct} (Ω) ^c	C_{dl} (mF cm ⁻²) ^d	ECSA (cm ⁻²) ^e
Fe@GC	400	94	2768	4.0	100
Fe ₂ P@APC	385	95	726	5.4	135

FeP@GPC	278	87	99	9.65	241.25
Fe ₂ P/FeP@GPC	333	90	200	6.35	158.75

a) Obtained from polarization curves of OER at the current density of 10 mA cm⁻² over the different as-synthesized materials;

b) Obtained from Tafel curves according to Tafel equation;

c) Obtained from the EIS results fitted with electrical equivalent circuit model;

d) Obtained from the linear graphs of Δj ($j_a - j_c$) at 1.05 V vs the scan rate, in which the slopes represent twice the values of C_{dl} ;

e) Estimated from the following equation: $ECSA = C_{dl}/C_s$;

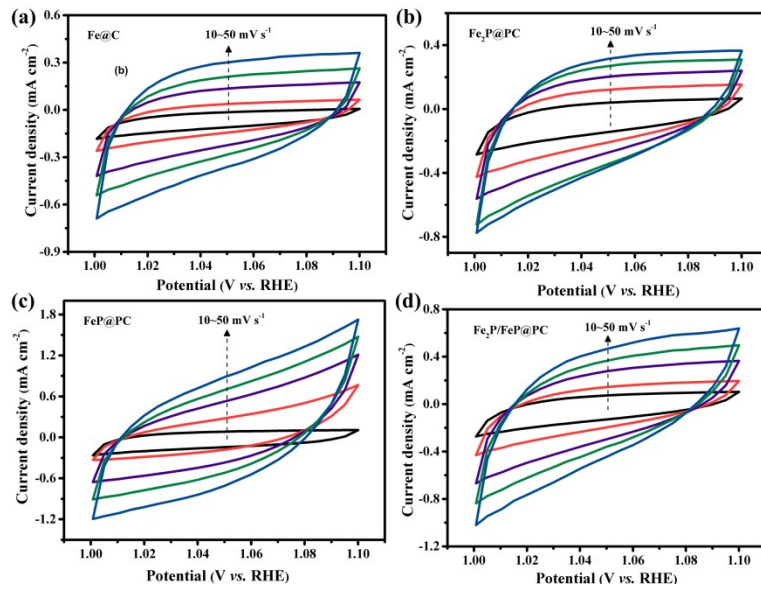


Figure S16. Cyclic voltammograms (CV) curves in 1 M KOH for (a) Fe@GC, (b) Fe₂P@APC, (c) FeP@GPC, (d) Fe₂P/FeP@GPC in the region of 1.0~1.10 V vs. RHE at various scan rates.

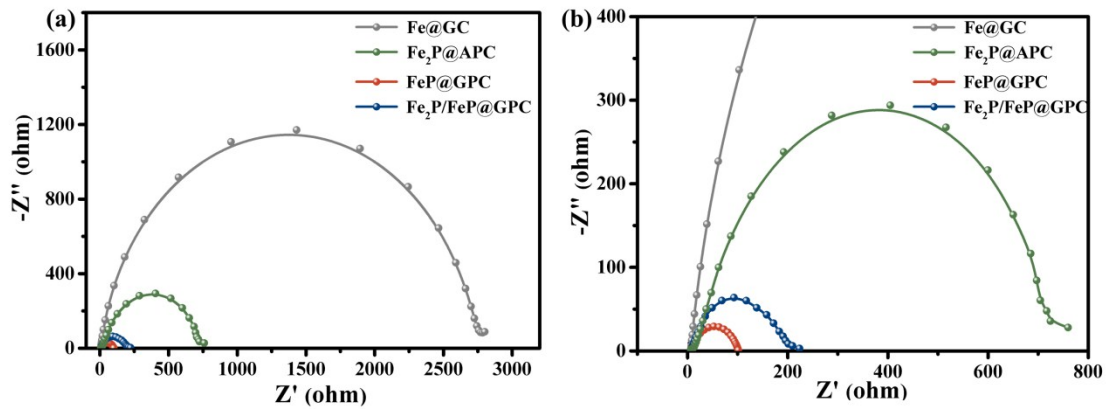


Figure S17. Nyquist curves derived from EIS measurements for OER in 1 M KOH.

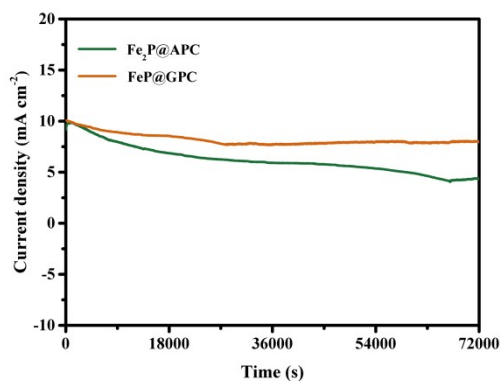


Figure S18. Chronoamperometric curves of as-synthesized Fe₂P@APC and FeP@GPC at applied constant overpotential of 385 mV and 278 mV vs RHE for 20h, respectively.

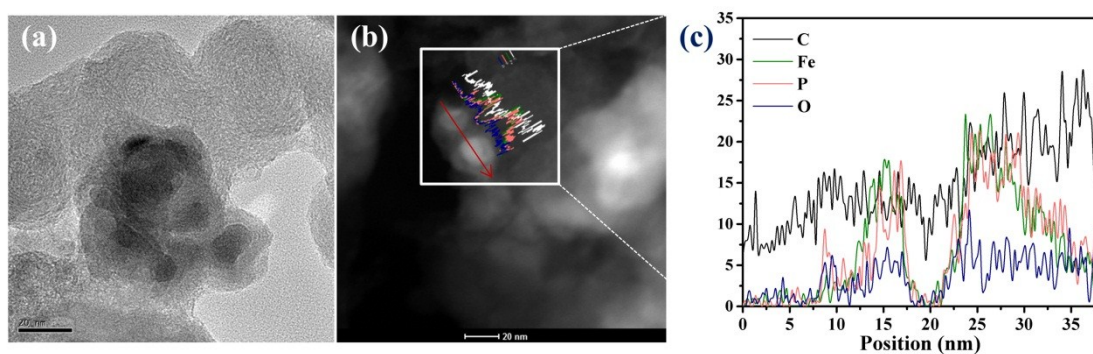


Figure S19. (a) (b) Bright- field and (c) Dark- field TEM images, (d) EDX line-scan profiles with Fe, P, C and O K shells of FeP@GPC catalyst after long time stability testing for OER in 1 M KOH.

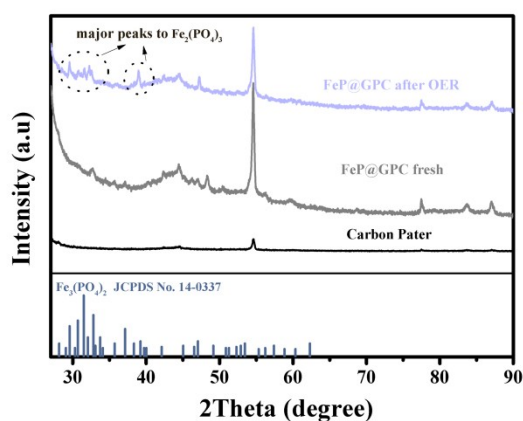


Figure S20. XRD results of FeP@GPC coating on carbon paper before and after long time stability testing for OER in 1 M KOH.

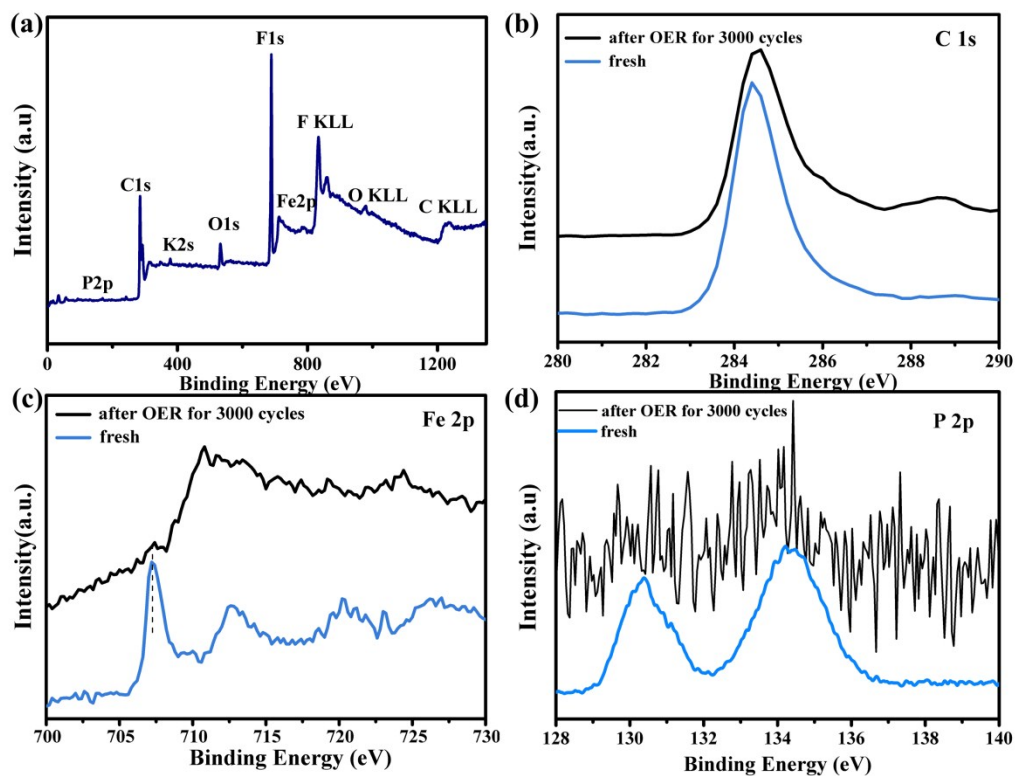


Figure S21. XPS results of FeP@GPC coating on carbon paper before and after long time stability testing for OER in 1 M KOH.

Supplementary Tables

Table S6. Summary of HER performance in 0.5 M H₂SO₄ electrolytes from the previous literatures. All the potentials are referred to RHE.

Catalyst	Substrate	Current density j (mA cm ⁻²)	η at the corresponding j (mV)	Ref.
		10	72	
FeP@GPC	Glassy carbon	20	93	This work
		100	150	
CoP@PNC	Glassy carbon	10	84	7
		10	89	
Cu ₃ P@NPPC	Glassy carbon	20	117	8
		80	207	
MoP@PC	Glassy carbon	10	258	9
		10	120	
Ni ₅ P ₄ -Ni ₂ P	Nickle Foam	20	140	10
		100	200	
Ni-P	Glassy carbon	10	98	11
		1	79	
Cu ₃ P	Copper Foam	10	143	13
		100	276	
Fe _x P@NPC	Glassy carbon	10	227	14
MoS ₂ /3D-NPC	Glassy carbon	10	210	15
Fe ₃ C/Mo ₂ C@NPGC	Glassy carbon	10	98	16
Co ₉ S ₈ -NSC@Mo ₂ C	Glassy carbon	10	74	17
MOF-CoSe ₂	Glassy carbon	80	330	18

Table S7. Summary of OER performances in 1 M KOH electrolyte from the previous literatures. All the potentials are referred to RHE.

Catalyst	Substrate	Current density		Ref.
		j (mA cm ⁻²)	η at the corresponding j (mV)	
		10	278	
FeP@GPC	Glassy carbon	20	302	This work
		100	408	
CoP@PNC	Glassy carbon	10	330	7
		10	320	
Ni ₂ P@NC	Glassy carbon	20	350	19
		40	370	
FeP@Au	Au-coated glass	10	320	20
Fe ₃ O ₄ @Co ₉ S ₈ /rGO	Glassy carbon	10	340	22
Co ₉ S ₈ @NOSC	Glassy carbon	10	340	23
FeP	Glassy carbon	10	350	24
NiCo/NiCoO _x	Glassy carbon	10	361	25
Co ₉ S ₈ -NSC@Mo ₂ C	Glassy carbon	10	293	17

References for Supplementary Information (SI) Section

1. S. Xie, J. Ye, Y. Yuan, Y. Chai and R. Yuan, *Nanoscale*, 2015, **7**, 18232-18238.
2. Y. Yuan, H. Pei, H. Chen, L. Zuo and J. Shen, *Catalysis Communications*, 2017, **100**, 202-205.
3. Y. Zheng, Y. Jiao, M. Jaroniec and S.-Z. Qiao, *Angewandte Chemie*, 2015, **54**, 52-65.
4. Y. Chen, H. Cao, W. Shi, H. Liu and Y. Huang, *Chemical Communications*, 2013, **49**, 5013-5015.
5. D. Li, Q. Liao, B. Ren, Q. Jin, H. Cui and C. Wang, *Journal of Materials Chemistry A*, 2017, **5**, 11301-11308.
6. R. Zhang, X. Wang, S. Yu, T. Wen, X. Zhu, F. Yang, X. Sun, X. Wang and W. Hu, *Advanced Materials*, 2017, **29**.
7. Z. Zhou, N. Mahmood, Y. Zhang, L. Pan, L. Wang, X. Zhang and J.-J. Zou, *Journal of Energy Chemistry*, 2017, **26**, 1223-1230.
8. R. Wang, X.-Y. Dong, J. Du, J.-Y. Zhao and S.-Q. Zang, *Advanced Materials*, 2018, **30**.
9. J.-S. Li, S. Zhang, J.-Q. Sha, H. Wang, M.-Z. Liu, L.-X. Kong and G.-D. Liu, *ACS Applied Materials & Interfaces*, 2018, **10**, 17140-17146.
10. X. Wang, Y.-V. Kolen'ko, X.-Q. Bao, K. Kovnir and L. Liu, *Angewandte Chemie*, 2015, **54**, 8188-8192.
11. X. Wang, W. Li, D. Xiong, D.-Y. Petrovykh and L. Liu, *Advanced Functional Materials*, 2016, **26**, 4067-4077.
12. D.-Y. Chung, S.-W. Jun, G. Yoon, H. Kim, J.-M. Yoo, K.-S. Lee, T. Kim, H. Shin, A.-K. Sinha, S.-G. Kwon, K. Kang, T. Hyeon and Y.-E. Sung, *Journal of the American Chemical Society*, 2017, **139**, 6669-6674.
13. J. Tian, Q. Liu, N. Cheng, A.-M. Asiri and X. Sun, *Angewandte Chemie*, 2014, **53**, 9577-9581.
14. Y. Cheng, J. Guo, Y. Huang, Z. Liao and Z. Xiang, *Nano Energy*, 2017, **35**, 115-120.
15. Y. Liu, X. Zhou, T. Ding, C. Wang and Q. Yang, *Nanoscale*, 2015, **7**, 18004-18009.
16. J.-S. Li, Y.-J. Tang, C.-H. Liu, S.-L. Li, R.-H. Li, L.-Z. Dong, Z.-H. Dai, J.-C. Bao and Y.-Q. Lan, *Journal of Materials Chemistry A*, 2016, **4**, 1202-1207.
17. X. Luo, Q. Zhou, S. Du, J. Li, J. Zhong, X. Deng and Y. Liu, *ACS Applied Materials & Interfaces*, 2018, **10**, 22291-22302.
18. J. Lin, J. He, F. Qi, B. Zheng, X. Wang, B. Yu, K. Zhou, W. Zhang, Y. Li and Y. Chen, *Electrochimica Acta*, 2017, **247**, 258-264.
19. Z. Pu, C. Zhang, I.-S. Amiinu, W. Li, L. Wu and S. Mu, *ACS Applied Materials & Interfaces*, 2017, **9**, 16187-16193.
20. J. Masud, S. Umaphathi, N. Ashokaan and M. Nath, *Journal of Materials Chemistry A*, 2016, **4**, 9750-9754.
21. J. Hou, Y. Sun, Y. Wu, S. Cao and L. Sun, *Advanced Functional Materials*, 2018, **28**, 1704447.
22. J. Yang, G. Zhu, Y. Liu, J. Xia, Z. Ji, X. Shen and S. Wu, *Advanced Functional Materials*, 2016, **26**, 4712-4721.
23. S. Huang, Y. Meng, S. He, A. Goswami, Q. Wu, J. Li, S. Tong, T. Asefa and M. Wu, *Advanced Functional Materials*, 2017, **27**, 1606585.
24. D. Xiong, X. Wang, W. Li and L. Liu, *Chemical Communications*, 2016, **52**, 8711-8714.
25. X. Yan, K. Li, L. Lyu, F. Song, J. He, D. Niu, L. Liu, X. Hu and X. Chen, *ACS Applied Materials & Interfaces*, 2016, **8**, 3208-3214.
26. E. Hu, Y. Feng, J. Nai, D. Zhao, Y. Hu and X.-W. Lou, *Energy & Environmental Science*, 2018, **11**, 872-880.